Available online at www.sciencedirect.com
ScienceDirect
Remote Sensing of Environment 107 (2007) 455–470
Remote Sensing of Environment
www.elsevier.com/locate/rse

Monitoring yield and fruit quality parameters in open-canopy tree crops under water stress. Implications for ASTER

G. Sepulcre-Cantó [a], P.J. Zarco-Tejada [a,*], J.C. Jiménez-Muñoz [b], J.A. Sobrino [b], M.A. Soriano [c], E. Fereres [a,c], V. Vega [d], M. Pastor [d]

[a] *Instituto de Agricultura Sostenible (IAS), Consejo Superior de Investigaciones Científicas (CSIC), Córdoba, Spain*
[b] *Universidad de Valencia, Valencia, Spain*
[c] *Dpto. de Agronomía, Universidad de Córdoba, Spain*
[d] *CIFA Córdoba, IFAPA, Junta de Andalucía, Spain*

Received 30 June 2006; received in revised form 21 September 2006; accepted 23 September 2006

Abstract

Work on water stress detection at tree and orchard levels using a high-spatial airborne thermal sensor is presented, showing its connection with yield and some fruit quality indicators in olive and peach commercial orchards under different irrigation regimes. Two airborne campaigns were conducted with the *Airborne Hyperspectral Scanner* (AHS) over olive and peach orchards located in Córdoba, southern Spain. The AHS sensor was flown at three different times on 25 July 2004 and 16 July 2005, collecting 2 m spatial resolution imagery in 80 spectral bands in the 0.43–12.5 μm spectral range. Thermal bands were assessed for the retrieval of land surface temperature using the *split-window* algorithm and TES (*Temperature-Emissivity-Separation*) method, separating pure crowns from shadows and sunlit soil pixels using the reflectance bands. Stem water potential and stomatal conductance were measured on selected trees at the time of airborne flights over the orchards. Tree fruit yield and quality parameters such as oil, weight and water content (for the olive trees), and fruit volume and weight (for the peach trees) were obtained at harvest and through laboratory analysis. Relationships between airborne-estimated crown temperature minus air temperature and stem water potential yielded $r^2=0.5$ (12:30 GMT) at the olive tree level, and $r^2=0.81$ (9:00 GMT) at the treatment level in peach trees. These results demonstrate that water stress can be detected at the crown level even under the usual water management conditions of commercial orchards. Regressions of yield and fruit quality against remote sensing estimates of crown temperature as an indicator of water stress, yielded $r^2=0.95$ (olive fruit water content) and $r^2=0.94$ (peach fruit mean diameter). These results suggest that high-spatial remote sensing thermal imagery has potential as an indicator of some fruit quality parameters for crop field segmentation and irrigation management purposes. A simulation study using ASTER spectral bands and aggregated pixels for stress detection as a function of irrigation level was conducted in order to study the applicability of medium resolution thermal sensors for the global monitoring of open-canopy tree crops. The determination coefficients obtained between the ASTER-simulated canopy temperature minus air temperature and stem water potential yielded $r^2=0.58$ (12:30 GMT) for olive trees, suggesting the potential for extrapolating these methods to ASTER satellite for global monitoring of open tree canopies.

Keywords: Water stress; Thermal; Fruit quality; Airborne; TES; AHS; ASTER; Remote sensing

1. Introduction

Water stress develops in crops when evaporative loss exceeds the supply of water from the soil (Slatyer, 1967). As a result of the decline in plant water status many physiological processes are affected, such as leaf expansion and other plant functions (Hsiao, 1973). Most crops are very sensitive to water deficits, and their yield may be negatively affected even by short-term water deficits (Hsiao et al., 1976).

* Corresponding author. Instituto de Agricultura Sostenible (IAS), Consejo Superior de Investigaciones Científicas (CSIC), Alameda del Obispo, s/n, 14004 — Córdoba, Spain. Tel.: +34 957 499 280, +34 676 954 937; fax: +34 957 499 252.
E-mail address: pzarco@ias.csic.es (P.J. Zarco-Tejada).
URL: http://www.ias.csic.es/pzarco (P.J. Zarco-Tejada).

0034-4257/$ - see front matter © 2006 Elsevier Inc. All rights reserved.
doi:10.1016/j.rse.2006.09.014

Leaf water potential (LWP) is commonly used to characterize plant water status, (Hsiao, 1990) but, in remote sensing studies, leaf water content is commonly used. Leaf water content is measured as the amount of water per unit leaf area, and several published studies demonstrate its successful estimation using remote sensing indices such as a water band index (WBI) (Peñuelas et al., 1993, 1997), moisture stress index (MSI) (Rock et al., 1986) or the normalized difference water index (NDWI) (Gao, 1996) among others. These indices are developed from near infrared (NIR) and shortwave infrared (SWIR) liquid water absorption bands. These studies have been conducted using spectroradiometers as a basis for future field-scale and aircraft/satellite-based measurements (Harris et al., 2005), using airborne sensors such as the Airborne Visible/Infrared Imaging Spectrometer (AVIRIS) (Serrano et al., 2000), and at global scales with the Moderate Resolution Imaging Spectroradiometer (MODIS) reflectance spectra and radiative transfer simulation models (Zarco-Tejada et al., 2003). Maps of leaf and canopy water content are important for agriculture and forestry (Gao & Goetz, 1995), drought assessments (Peñuelas et al., 1993), and susceptibility to fire (Ustin et al., 1998).

Although water content in vegetation canopies can be assessed by remote sensing, leaf water potential is a more precise indicator of the plant water status for predicting effects of water deficits on crop yields because small changes in the relative water content of leaf tissues corresponds to large changes in leaf water potential (Acevedo et al., 1979; Kramer & Boyer, 1995). Changes in leaf water content that may be easily detectable normally occur at advanced stages of dehydration, being therefore a parameter of limited interest for predicting crop water status for situations where high crop productivity levels are sought. Even though there is interest in obtaining leaf water potential information, it is often suggested that pre-dawn measurements of leaf water potential are the most accurate estimate soil moisture status (Cowan, 1965; Slatyer, 1967) but the inconvenience and narrowness of time window makes this measurement impractical. The dynamics of the daily course of leaf water potential (LWP) makes it difficult to determine the appropriate time of measurement; however, LWP in sunny days is relatively constant for several hours around solar noon, the time when it reaches its minimum value (Kramer & Boyer, 1995). Shackel et al. (1997) have found that stem water potential (SWP) is more reliable than leaf water potential as an indicator of plant water status in a number of tree crops. At any rate, the labour involved, together with the limitations outlined above, limits the number of water potential observations that can be made (Stimson et al., 2005). When the plant is stressed and transpiration decreases, the crop canopy temperature tends to rise appreciably because of the reduction in evaporative cooling. This is the basis for the approach of sensing crop stress by monitoring canopy temperature with thermal infrared radiation (Idso et al., 1981; Jackson et al., 1981, 1977) proposing the crop water stress index (CWSI). This technique has been widely studied and developed mainly at ground level using hand-held thermal infrared thermometers (Idso et al., 1978; Jackson & Pinter, 1981; Jackson et al., 1977) and, more recently, using thermal scanners (Wanjura et al., 2004) and thermal cameras (Cohen et al., 2005; Leinonen & Jones, 2004).

Some studies have focused in the combination of vegetation indices and surface temperature, proposing the water deficit index (WDI) (Moran et al., 1994) for satellite image studies. Recent studies use the relationship between vegetation indices and surface temperature at regional scales for assessment of vegetation condition and water stress using satellite imagery (Jang et al., 2006). At the airborne level, recent work has shown the detection of water stress at in a closed cotton canopy (Detar et al., 2006).

Despite the potential usefulness of remote sensing for thermal detection in vegetation canopies, studies where thermal imagery is used for water stress detection are limited, in particular for open canopies such as tree crops. There is a lack of sensors onboard satellite platforms with optimal spatial resolution to monitor orchard crops at the tree scale (i.e. ideally 0.5 to 2 m spatial resolution in the thermal region). Even in the case of high-spatial resolution imagery collected from airborne sensors, shadows and direct soil influences involve problems in the canopy temperature retrieval due to the canopy heterogeneity characteristic in orchard canopies. Nevertheless, recent studies on surface temperature estimation with high-spatial resolution remote sensing imagery have proved that this technology is available for obtaining accurate measurements of surface temperature. Different methods can be used to retrieve land surface temperature from thermal infrared data provided by only one or two thermal bands, as for example the single-channel methods or the split-window technique. Land surface temperature and emissivity can be also obtained from multispectral thermal data using the Temperature and Emissivity Separation (TES) algorithm (Gillespie et al., 1998). A detailed review of methods can be found in Sobrino et al. (2002), Dash et al. (2002) and Kerr et al. (2004). The feasibility of these methods for retrieving land surface temperature from ten thermal-infrared bands of the *Airborne Hyperspectral Scanner* (AHS) is assessed in Sobrino et al. (2006). In this study root mean square errors of 1.4 K were obtained for olive tree canopy temperature. In addition, Sepulcre-Cantó et al. (2006) demonstrated in olive orchards that the AHS high-spatial resolution imagery enabled the study of spatial and temporal thermal effects of water stress at tree and orchard levels.

It has been long known that water stress affects not only fruit yield but also, fruit quality (Fereres et al., 2003; Uriu & Magness, 1967). In the case of olive and peach trees, Moriana et al. (2003) and Girona et al. (2003) have shown the effects of sub-optimal irrigation on fruit yields. Deficit irrigation research in orchard crops aims at saving irrigation water, while increasing or maintaining income, even if yield is affected (reviewed by Fereres & Soriano, in press). To implement deficit irrigation strategies, precise detection and monitoring of water stress is essential. Thus, the detection of small thermal differences (0.5 to 2 K), if associated with water-deficit stress levels in orchard crops at the tree level, could be a very useful detection and monitoring technique to manage deficit irrigation. The work presented here focuses on the detection of tree-crown temperature differences as affected by water stress in a commercial peach orchard under several deficit irrigation levels. Previous studies were conducted under more severe water stress conditions that effected large differences in olive canopy temperature (Sepulcre-Cantó et al., 2006). The work

Table 1
Irrigation treatments applied over each the study site in 2004 and in 2005 campaigns

Study site	Treatment label	Doses applied	Period of application
Olive trees (thermal validation)	R	100% ET	From mid-June to mid-October
	S1	25% ET	From mid-June to mid-October
	S2	43% ET	From mid-June to the first week of July and from the first week of September to mid-October
		Not irrigated	From the first week of July to the first week of September
Olive trees (yield and quality measurements)	I	100% ET	From mid-June to mid-October
	II	50% ET	From the first week of July to mid-September
		100% ET	From mid-June to the first week of July and from mid-September to mid-October
	III	25% ET	From the first week of August until mid-September
		100% ET	From mid-June to the fist week of August and from mid-September to mid-October
	IV	100% ET	From mid-June to mid-July and from mid-September to mid-October
		Not irrigated	From mid-July to mid-September
Peach trees	A	Non irrigated	From the fist week of May to the fist week of July and from mid-August to mid-September
		200% ET	From the last week of June to mid-July*
		100% ET	From half July to mid-August.
	B	67% ET	From the first week of may to mid-September
	C	100% ET	From the first week of may to mid-September
	D	133% ET	From the first week of may to mid-September.

*Beginning of the Stage III of fruit growth (Mitchell & Chalmers, 1982).

here aims at detecting small differences in canopy temperatures under both extreme and commercial orchard irrigation conditions, and to assess their potential for tree-level water stress detection in relation to olive and peach fruit yield and quality. We present also work on the potential for extrapolating these methods to ASTER satellite for monitoring orchard canopies at larger scales.

2. Materials and methods

2.1. Study sites

The ground truth datasets and aircraft images were acquired in two different orchards (an experimental olive orchard and a commercial peach orchard) located in Córdoba, southern Spain (37° 48′ N, 4° 48′ W) in summer 2004 and 2005. The climate of the area is Mediterranean with an average annual rainfall of 650 mm, concentrated from autumn to spring, and a reference annual evapotranspiration (ETo) of 1390 mm. The olive orchard (*Olea europaea* L cv. 'Arbequino') used for the experiment has an extension of 4 ha, and was planted in 1997 in a 7 m × 3.5 m pattern (408 trees ha^{-1}). The mean crown size of the olive trees was 50 m^3 (approximately with a spherical crown shape) with 6 m of height. Drip irrigation method was used for supplying accurate water doses at tree level. The water stress study and thermal imagery validation was conducted over an area of 6 rows of 18 olive trees (2646 m^2) where three drip irrigation treatments were randomly applied (Table 1). A detailed description of blocks size and irrigation treatments in this experimental orchard can be found in Sepulcre-Cantó et al. (2006). Yield and olive fruit quality measurements were conducted over an area of 15

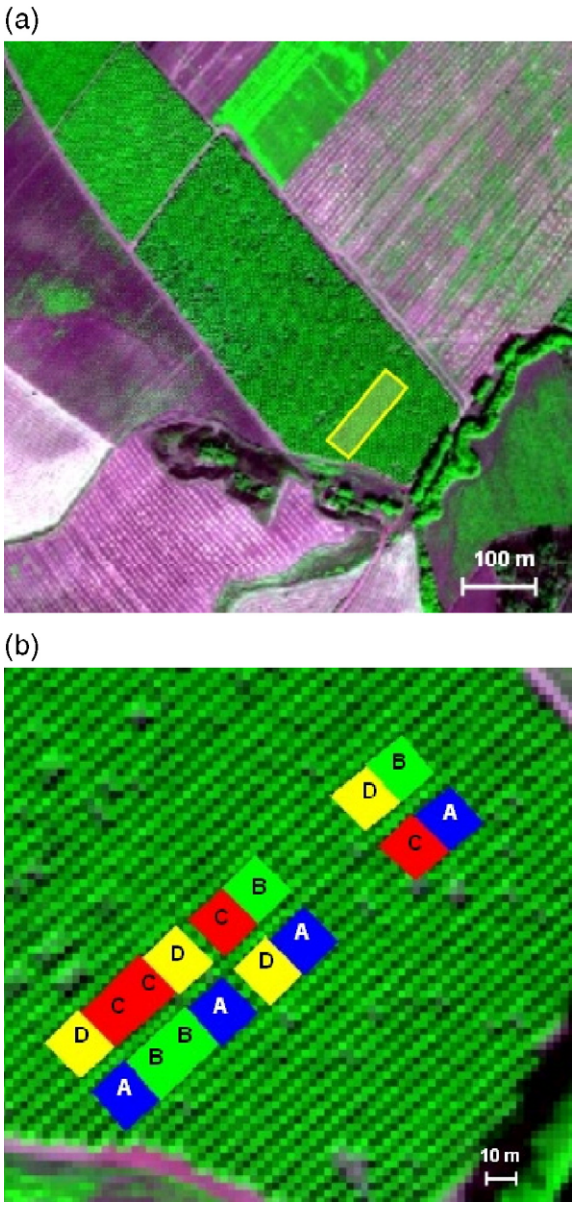

Fig. 1. (a) Image of the peach orchard acquired on 16 July 2005 with the Airborne Hyperspectral Scanner (AHS). The study area used is shown under a yellow square. (b) A close up of the study area where the squares represent the experimental plots of trees under the same irrigation treatment. The band used for the false colour images were: band 2 (λ = 475 nm) for blue colour, band 9 (λ = 685 nm) for red colour, and band 12 (λ = 0.775 nm) for green colour.

rows of 24 olive trees (360 trees; 8820 m^2) where four drip irrigation treatments were applied (Table 1). These irrigation treatments were designed as part of deficit irrigation trials conducted in the orchard.

The second study site is in a commercial peach orchard (*Prunus persica* L., cv. 'Baby Gold') with an extension of 3 ha, grown on a loam soil. The orchard was planted in 1993 with trees at 5 m × 3.25 m with rows oriented in the N–S direction. The mean crown size of the peach trees (approximately with a spherical shape) was 25 m^3 with 4 m of height. Each experimental plot had 12 trees, out of which only the central two trees were monitored. The soil had a cover crop that was mowed frequently. Four drip irrigation treatments (Table 1) replicated four times were applied within an area of 6 rows of 32 peach trees each (3120 m^2) (Fig. 1).

2.2. Field data collection

During the summer of 2004 and 2005, olive tree temperature was monitored. Infrared sensors covering the 6.5–14 μm range (model IRTS-P, Apogee, Utah, USA) were placed over 10 trees comprising the three irrigation treatments (Sepulcre-Cantó et al., 2006), recording the mean temperature at 5-minute intervals in 3 dataloggers (model CR10X, Campbell Sci., UT, USA). A thermal camera (Snapshot, Infrared Solutions Inc., MN, USA) was used to acquire thermal images from olive trees under different irrigation treatments at 15:00 GMT during summer 2004. In addition, a hand-held thermal radiometer (model Raynger II, Raytek, California, USA) with a single broadband covering the range 8-14 μm was used to measure tree temperatures at 12:00 GMT from olive trees (in summer 2004 and 2005), and from peach trees (in summer 2005). Air temperature (Ta) was continuously measured in the field with a Vaisala Weather Transmitter (model WXT510, Vaisala Oy, Helsinki, Finland) installed in the olive orchard at 1 m over a control tree (6 m above ground). In the peach orchard, air temperature values were obtained from an automated meteorological station located at 1 km from the orchard.

A pressure bomb (PWSC Model 3000, Soilmoisture Equipment Corp., California, USA) was used to measure stem water potential (SWP; Shackel et al., 1997) from 11 olive trees covering the 3 irrigation treatments, measuring weekly at 12:00 GMT. Similarly, SWP from the peach trees was measured weekly at 12:00 GMT. This was done for all 32 trees covering the 4 irrigation treatments. In addition, stomatal conductance (Gl) in the olive orchard was measured once a week at 10:00 GMT from 3 trees with a leaf steady-state porometer (model PMR-4, PP Systems, Hitchin Herts, Great Britain). These measurements (SWP and Gl) were conducted from July to October in 2004 and 2005.

2.3. Remote sensing airborne campaigns

Two airborne campaigns were conducted by the Spanish Aerospace Institute (INTA) with the Airborne Hyperspectral Scanner (AHS) (developed by Sensytech Inc., currently Argon St Inc., USA). Flights over the olive orchard were made on 25 July 2004 and on 16 July 2005 at 7:30, 9:30 and 12:30 GMT, in order to study changes in water stress over the course of the day as function of the irrigation treatments applied. Flights over the peach orchard were made at 9:00 GMT in 2004, and at 9:00 and 13:00 GMT in 2005.

The AHS sensor has 80 spectral bands in the 0.43 μm to 12.5 μm spectral range. The 80 bands are distributed in 4 ports (VIS/NIR, SWIR, MWIR and TIR). The sensor has a 90° FOV and a 2.5 mrad instantaneous field of view (IFOV). The aircraft flew at 1000 m altitude above ground level (AGL), obtaining 6000 × 2000 m^2 images at 2 m spatial resolution. The flight paths were kept in the solar plane and designed so that the study orchard was in the centre of the images. Imagery was processed applying geometric, radiometric and atmospheric corrections. Image atmospheric correction was done using the MODTRAN-4 radiative transfer code (Berk et al., 1999) and in situ radiosoundings launched at 7:00 and 12:00 GMT on 16 July 2005. A full description of the AHS bands calibration and the radiometric and the atmospheric correction process can be found in Sobrino et al. (2006).

In the 2005 campaign, a detailed study on water potential as a function of time was conducted, measuring stem water potential from 18 trees and stomatal conductance from 12 trees simultaneous to the three overflight times over the olive orchard. During both 2004 and 2005 campaigns, SWP of the peach trees was measured four days previous to the airborne acquisitions.

2.4. Airborne temperature retrieval and ASTER simulation

Land surface temperature (LST) was retrieved from AHS thermal infrared data acquired in 2004 and 2005 using the split-window algorithm described in Sepulcre-Cantó et al. (2006):

$$\begin{aligned} T_s = {} & T_{75} + 0.4850(T_{75}-T_{79}) + 0.0068(T_{75}-T_{79})^2 \\ & + 0.0798 + (47.15-10.80W)(1-\varepsilon) \\ & + (-49.05 + 21.53W)\Delta\varepsilon \end{aligned} \quad (1)$$

where T_s is the LST (in K), T_{75} and T_{79} are the *at-sensor* brightness temperatures (K) of the AHS thermal bands 75 (10.069 μm) and 79 (12.347 μm), $\varepsilon = (\varepsilon_{75} + \varepsilon_{79})/2$ and $\Delta\varepsilon = (\varepsilon_{75} - \varepsilon_{79})$ are the mean effective emissivity and the emissivity difference, and W is the total atmospheric water vapour content (g cm^{-2}). In addition, the TES algorithm adapted to AHS data (Sobrino et al., 2006) was also applied to the imagery acquired in 2005, because this method requires an accurate atmospheric correction and atmospheric soundings that were launched near to the AHS overpass only in 2005. According to the results presented in Sepulcre-Cantó et al. (2006) and Sobrino et al. (2006), LST can be retrieved from AHS data with root mean square errors (RMSE) lower than 1.5 K.

In order to study the feasibility of using medium resolution satellite sensors such as ASTER (90 m spatial resolution) for water stress detection in open-tree canopies, a degradation of the spatial resolution was conducted to assess the effects of crown-shadow–soil temperature aggregation on 90 m pixels, as well as the spectral characteristics of the ASTER sensor on-board TERRA satellite. The ASTER sensor has 5 thermal bands in the 8–12 μm spectral region from 10 to 14, with spectral

ranges of 8.125–8.475, 8.475–8.825, 8.925–9.275, 10.25–10.95 and 10.95–11.65 μm (Abrams, 2000; Yamaguchi et al., 1998). The scaling study was conducted using the radiative transfer equation applied to the thermal infrared spectral region and to a certain sensor band (i):

$$L_{\text{sensor},i} = [\varepsilon_i B_i(T_s) + (1-\varepsilon_i)L_i^{\downarrow}]\tau_i + L_i^{\uparrow} \quad (2)$$

where L_{sensor} is the radiance measured by the sensor, ε; and T_s are the surface emissivity and temperature respectively, τ is the atmospheric transmissivity, $L^{\uparrow}$ is the up-welling path radiance, $L^{\downarrow}$ is the down-welling sky irradiance divided by π, and $B_i(T_s)$ is the channel radiance which would be measured if the surface was a blackbody ($\varepsilon = 1$) at temperature T_s, defined by the Planck law (Eq. (3)).

$$B_i(T_s) = \frac{C_1}{\lambda_i^5\left[\exp\left(\frac{C_2}{\lambda_i T_s}\right)-1\right]} \quad (3)$$

with $C_1 = 1.19104\times10^8$ W μm^4 m^{-2} sr^{-1}, $C_2 = 14387.7$ μm K, and λ_i the effective wavelength (in μm) defined as in Eq. (4):

$$\lambda_i = \frac{\int_0^{\infty} \lambda f_i(\lambda)\mathrm{d}\lambda}{\int_0^{\infty} f_i(\lambda)\mathrm{d}\lambda} \quad (4)$$

in which $f_i(\lambda)$ is the spectral response of the sensor in channel i.

Eq. (2) was used to simulate the at-sensor radiance (L_{sensor}) for each ASTER thermal band. For this purpose, the land surface temperature (T_s) and emissivity (ε) obtained from the AHS data at 2 m spatial resolution sensor was used. Simulated ASTER emissivities were estimated using linear relationships between ASTER and AHS band emissivities, which were obtained from a dataset of emissivity spectra extracted from the ASTER spectral library (http://speclib.jpl.nasa.gov). The atmospheric parameters (τ, $L^{\uparrow}$, $L^{\downarrow}$) were obtained from the atmospheric soundings and the MODTRAN-4, using the filter functions of the ASTER bands. Then, the simulated ASTER at-sensor radiance at 2 m spatial resolution was aggregated to simulate pixels of 15×20 m^2 spatial resolution comprising 12 trees under the same irrigation treatment. This simulation study, using the same ASTER spectral bands and aggregated pixels for stress detection as function of irrigation level, would assess the applicability of medium resolution thermal sensors for the global monitoring of open-canopy tree crops.

Table 2
Stem water potential (SWP) and stomatal conductance (Gl) measured at the beginning of the irrigation period (first of May for the peach trees, and at the end of June for the olive trees), and the values measured in the period of maximum stress (to mid September)

	Irrigation treatments	Beginning of the irrigation period		Period of maximum water stress	
		SWP (MPa)	Gl (mm s^{-1})	SWP (MPa)	Gl (mm s^{-1})
Olive trees	S1 (1/4 ET)	−1.4	4.7	−3.5	1.5
	S2 (1/4 ET)	−1.1	13.7	−3.1	3.0
	R (ET)	−0.9	13.0	−1.2	5.0
Peach trees	A (2/3 ET)	−0.35	–	−1.7	–
	B (2/3 ET)	−0.35	–	−1.5	–
	C (ET)	−0.35	–	−1.2	–
	D (4/3 ET)	−0.35	–	−0.8	–

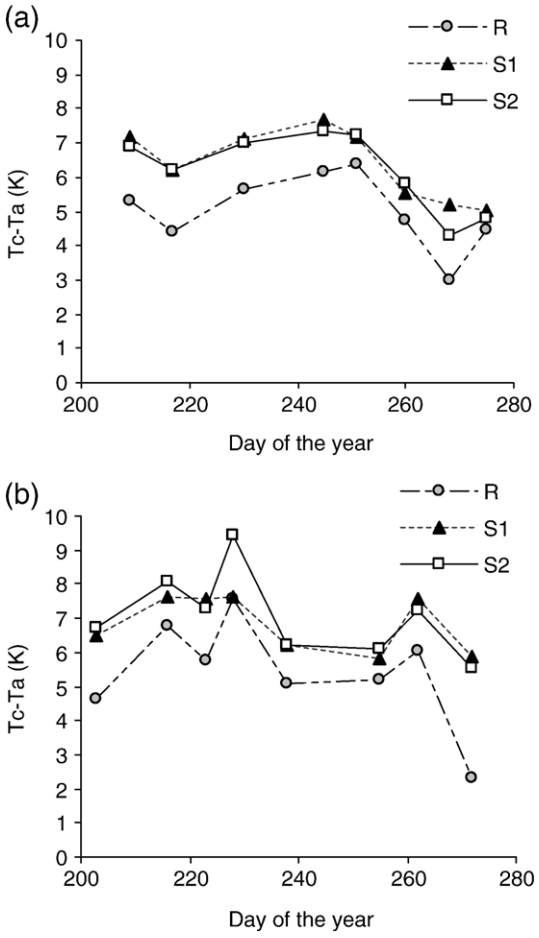

Fig. 2. Differences between canopy (Tc) and air (Ta) temperature (K) for the different irrigation treatments obtained with a hand-held infrared thermometer at 12:00 GMT from olive trees: (a) in the 2004 summer campaign and (b) in the 2005 summer campaign.

2.5. Yield and fruit quality parameters data

The harvest of the olive trees was conducted using a mechanical shaker. All the olives harvested from each tree were weighed for to obtain olive yield (fresh weight, kg tree^{-1}), and a representative sample of 2 kg was selected for the analysis. The oil content in the fresh fruit (oil weight per fresh weight, g g^{-1}) was determined by nuclear magnetic resonance (Hidalgo & Zamora, 2003), and oil yield (kg tree^{-1}) was calculated as the product of olive yield by oil content in the fresh fruit. Fruit water content was obtained drying a sub-sample in an oven until constant weight, and oil content was standardized with respect to the dry weight.

In the peach orchard, trees were harvested manually in three times to optimise ripening. All the fruits of the 32 monitored trees were counted and weighted in the field at each harvest, and all the fruit diameters were measured. Total peach yield, fresh fruit weight and fruit diameter were determined. The total soluble solids content (TSS) of each monitored peach tree was obtained at each harvest in a representative sample of ten fruits, using a digital calibrated refractometer (model ATC-1E, Atago

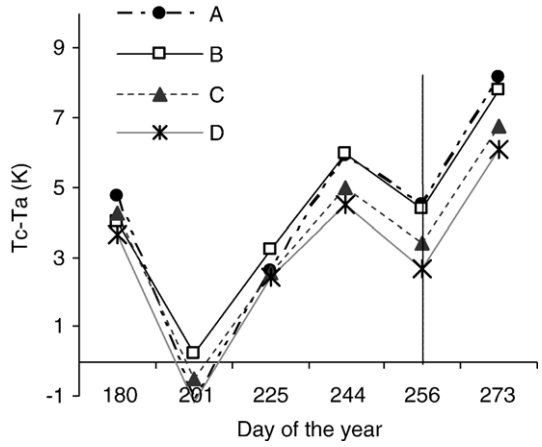

Fig. 3. Differences between canopy (Tc) and air (Ta) temperature (K) for the different irrigation treatments obtained with a hand-held infrared thermometer at 12:00 GMT from peach trees in the 2005 summer campaign. Irrigation period ended on 13 September (day 256, dashed line).

C., Tokio, Japan). The final values of fruit weight, fruit diameter and total soluble solids content were the weighted average for the three harvests.

3. Results and discussion

3.1. Field measurements for water stress detection

The stem water potential (SWP) and stomatal conductance (Gl) measurements in the olive orchard reflected the treatment differences in water supply in 2005 (Table 2). The values obtained for SWP and Gl were lower in the trees under deficit irrigation treatments, showing an increment in the differences between treatments as the season went on. These results agreed with those obtained during the previous year, on the summer 2004 campaign (Sepulcre-Cantó et al., 2006). In the peach orchard in 2005, SWP exhibited trends that were similar to those observed in the olive orchard (Table 2), although the SWP values were much higher in peach than in olive trees. The same occurred in 2004 when measurements varied from −0.35 MPa for all treatments at the beginning of the irrigation season to −0.8 MPa for D treatment and −0.9 MPa for C (farm) treatment, and −1.3 MPa for B and A treatments at the moment of maximum water stress (end of the irrigation).

The difference between canopy (Tc) and air (Ta) temperature obtained for the different irrigation treatments using the hand-

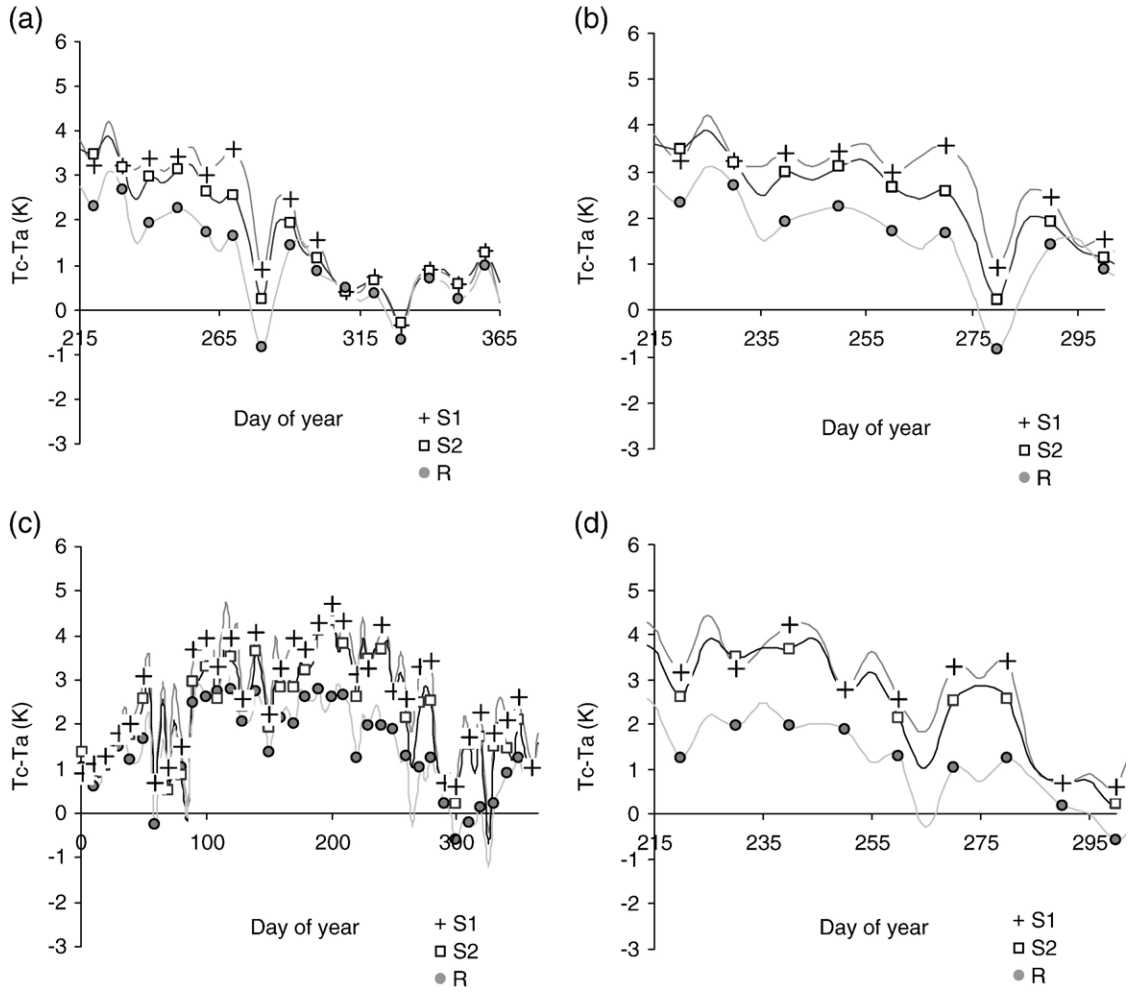

Fig. 4. Yearly Tc−Ta (K) differences at 14:00 GMT for the different olive irrigation treatments. Tc and Ta were measured with the infrared thermal sensors placed on top of the olive trees. a) From July to December 2004, b) data for the summer 2004, c) from January to December 2005, and d) data for summer 2005.

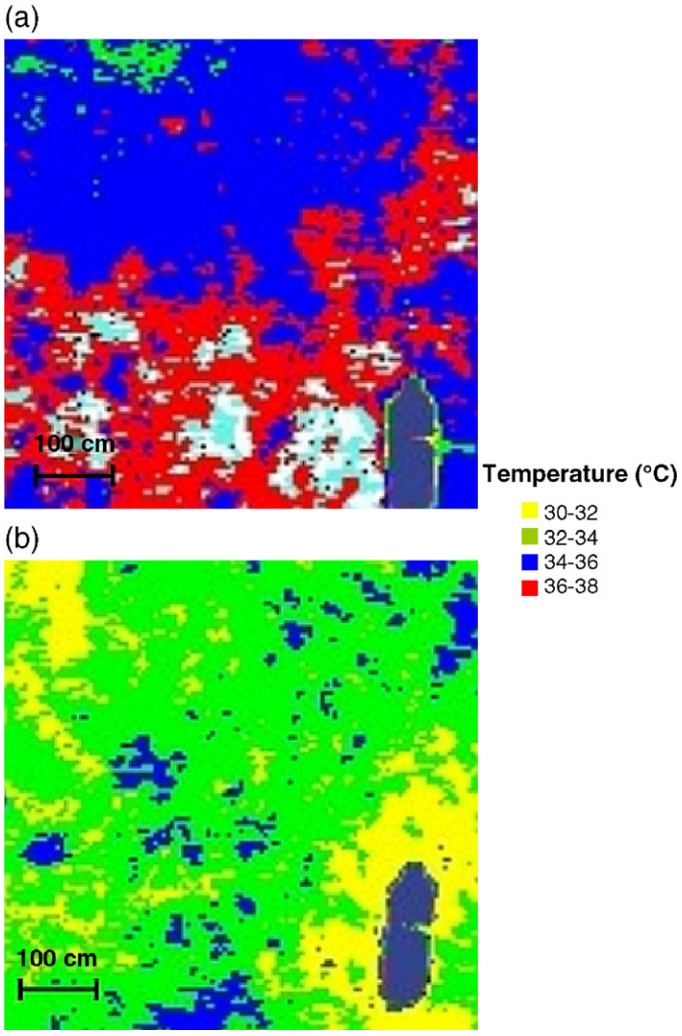

Fig. 5. Thermal images of: a) a deficit irrigation olive tree canopy and b) a well watered olive tree canopy.

held infrared thermometer are shown in Fig. 2 for olive trees and in Fig. 3 for peach trees. In both cases, olive and peach trees, Tc–Ta differences consistently varied with the applied irrigation treatments. The tree Tc–Ta values were greater under deficit irrigation than in the well irrigated treatments. Treatment differences were less in the case of the peach trees because the level of water stress imposed in a commercial orchard was much less than that applied in the olive experiment, as indicated by the SWP values (Table 2). The Tc–Ta values obtained for the olive trees at half of September were 7.2 K for S1 and S2 treatment, and 6.4 K for R treatment in 2004; and 5.8 K for S1 treatment, 6.1 K for S2 treatment, and 5.2 K for R treatment in 2005 (Fig. 2a, b). Peach-tree temperature measured with the hand-held thermal sensor during the 2005 summer campaign (Fig. 3) showed differences between Tc–Ta of 4.4 K for treatment A and 4.3 for treatment B trees at half of September, while Tc–Ta yielded 3.3 K for trees under the farm schedule (treatment C) and 2.5 K for trees under D treatment (4/3 ET).

Top-of-the-canopy and air temperature were monitored continuously with infrared sensors and a Vaisala throughout the years 2004 and 2005 on olive trees. The maximum temperature differences between treatments were observed at 14:00 GMT, although the Tc–Ta values for the different irrigation treatments were lower than those obtained at 12:00 GMT. The Tc–Ta time series at 14:00 GMT are presented in Fig. 4 for July to December 2004, and for January to December 2005. Differences between treatments can be observed from June to November, detecting the recovery after the first autumn rainfall in November 2004 and 2005. Tc–Ta yielded 4 K for trees under deficit irrigation treatment S1 in the period of maximum stress (from August to October), while Tc–Ta yielded 2 K for trees under R treatment in 2004 and in 2005.

In addition, field measurements with a thermal camera were conducted in summer 2004, acquiring thermal images of the olive crowns under different irrigation treatments (Fig. 5). Differences between crown temperatures as a function of the applied water deficits were detected, furthermore demonstrating a greater thermal homogeneity for the crown temperature in well-watered trees. The canopy temperature variability was proposed by Clawson and Blad (1982) to signal the onset of plant water stress in corn but there are not studies applying this methodology to trees. Thermal images acquired with the thermal camera were compared with the hand-held infrared radiometer and with infrared sensors placed on top of the tree to asses the validity of the crown-thermal imagery measurements as an indicator of the mean crown temperature for the tree. The values compared were the mean lateral temperature of the crown obtained from the thermal imagery with the mean top of the crown temperature measured with the infrared sensors and the lateral point-measurement of the crown temperature made with the thermal gun, all the instruments measuring at the same time. The images of the trees under deficit irrigation treatments showed higher temperatures than images of well irrigated trees (Table 3). The mean crown temperature per treatment obtained from the thermal camera imagery on 4 October 2004 for trees under deficit irrigation treatment S1 was 35.1 °C (standard deviation of 1.3 °C) for a measured SWP of −2.8 MPa, while the mean crown temperature obtained for trees under irrigation treatment R was 33.0 °C (standard deviation of 1.2 °C) for a measured SWP of −1.2 MPa (Table 3). Fig. 6 (a,b) show the relationships between the temperature obtained with the thermal camera imagery, and the temperature measured with the hand-held thermometer ($r^2=0.44$) (Fig. 6a) and with the infrared sensors placed on top of the trees ($r^2=0.59$) (Fig. 6b) on 4 October 2004. The relationships obtained in the field between stem water potential and the crown temperature obtained from

Table 3
Stem water potential, and mean olive crown temperature measured with the hand-held thermometer and obtained from the thermal camera imagery, with its standard deviation values (SD), obtained from olive trees on 4 October 2004

Treatment	Stem water potential (MPa)	Olive crown temperature (°C)		
		Infrared radiometer	Thermal image	Image SD
R	−1.19	34.4	33.0	1.2
S2	−1.69	34.4	34.0	1.2
S1	−2.84	35.7	35.1	1.3

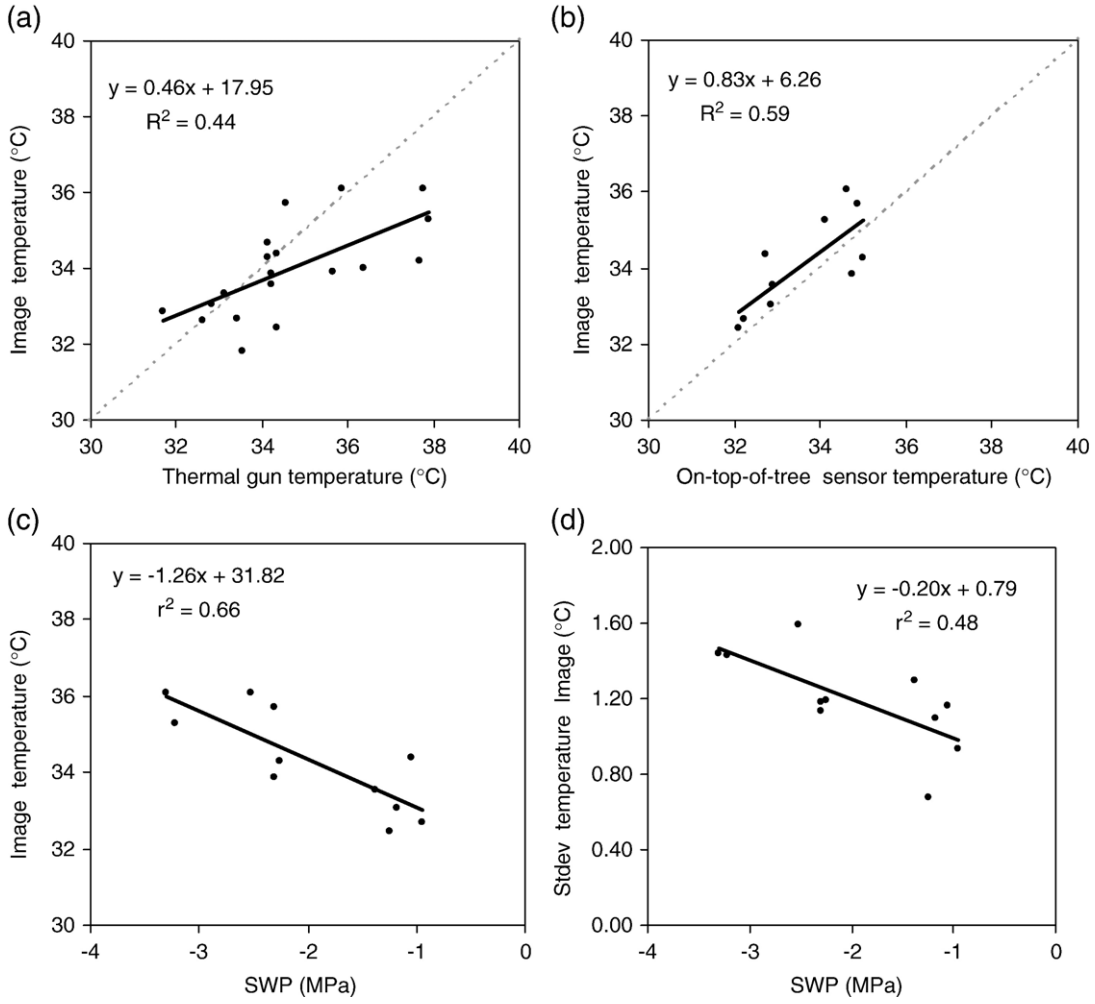

Fig. 6. Relationship between crown temperatures obtained from the thermal camera imagery, and measured with: a) the hand-held thermometer and b) with the infrared sensors placed on top of the olive trees, in the olive orchard on 4 October 2004. c) Relationship between temperature obtained from the thermal camera imagery and stem water potential (SWP). d) Relationship between stem water potential (SWP) and the standard deviation of the canopy temperature obtained from the thermal camera imagery.

the thermal camera imagery (Fig. 6c) demonstrate the successful use of the thermal camera imagery as indicator of water stress at the tree level. Moreover, the standard deviation of the crown temperature obtained with the camera imagery indicates the level of heterogeneity for the crown canopy temperature as function of the water stress level. This is consistent with the determination coefficient of $r^2 = 0.48$ obtained between standard deviation of the imagery and stem water potential (Fig. 6d).

3.2. Detection of irrigation levels in olive and peach orchards from airborne thermal imagery

Temperature values per irrigation treatments obtained from airborne AHS imagery at 2 m spatial resolution for 2004 and 2005 campaigns are presented in Table 4 for olive trees and in Table 5 for peach tress. Airborne remote sensing-derived estimates for Tc and Tc–Ta for each orchard tree and irrigation treatment are

Table 4
Temperature (Tc) and differences between canopy and air temperature (Tc–Ta) for olive irrigation treatments, obtained by means of the airborne AHS sensor at 3 different times on 25 July 2004 and on 16 July 2005. S1 and S2 are two deficit irrigation treatments and R indicates the well irrigated treatment

Year	Time (GMT)	Tc (K)			Tc–Ta (K)		
		S1	S2	R	S1	S2	R
2004	7:30	303.5±0.1	303.5±0.4	303.0±0.2	1.1±0.1	1.1±0.4	0.6±0.2
	9:30	309.8±0.3	309.7±0.5	309.0±0.2	1.7±0.3	1.6±0.5	0.9±0.2
	12:30	315.4±0.6	315.0±0.3	314.4±0.4	3.3±0.6	2.9±0.3	2.3±0.4
2005	7:30	299.9±0.2	299.7±0.5	299.1±0.2	1.8±0.2	1.7±0.5	1.1±0.2
	9:30	306.1±0.5	306.0±1.0	304.6±0.6	3.5±0.5	3.3±1.0	2.1±0.6
	12:30	317.1±0.5	317.0±1.0	315.2±0.7	4.1±0.5	4.0±1.0	2.3±0.7

Table 5
Temperature differences (Tc–Ta) obtained between canopy (Tc) and air temperature for the different irrigation treatments (A, B, C and D) in peach, obtained by means of the AHS sensor at different overflight times on 25 July 2004 and on 16 July 2005

Year	Time (GMT)	Tc (K)				Tc–Ta (K)			
		A	B	C	D	A	B	C	D
2004	9:00	307.4±0.2	307.6±0.4	307.4±0.3	307.1±0.7	0.7±0.2	1.1±0.4	1.3±0.3	1.0±0.7
2005	9:00	301.6±0.2	302.2±0.3	301.7±0.3	301.4±0.4	2.1±0.2	2.6±0.3	2.1±0.3	1.9±0.4
	13:00	312.0±1.0	313.0±1.0	312.4±0.9	312.0±1.0	3.0±1.0	4.0±1.0	3.6±0.9	3.0±1.0

consistent with the measurements conducted in the field. The olive trees under well irrigated treatments showed lower temperature values than trees under deficit irrigation treatments, for the three overflight times (Table 4). Differences between deficit and well irrigated treatments yielded 1 K and 2 K at 12:30 GMT in 2004 and 2005, respectively. Tc–Ta yielded 3 K and 4 K for the trees under deficit irrigation treatment S1 at 12:30 GMT in 2004 and 2005, respectively, while trees under well irrigated treatment maintained 2 K difference (Table 4). Similarly, for the peach orchard temperature differences between extreme irrigation

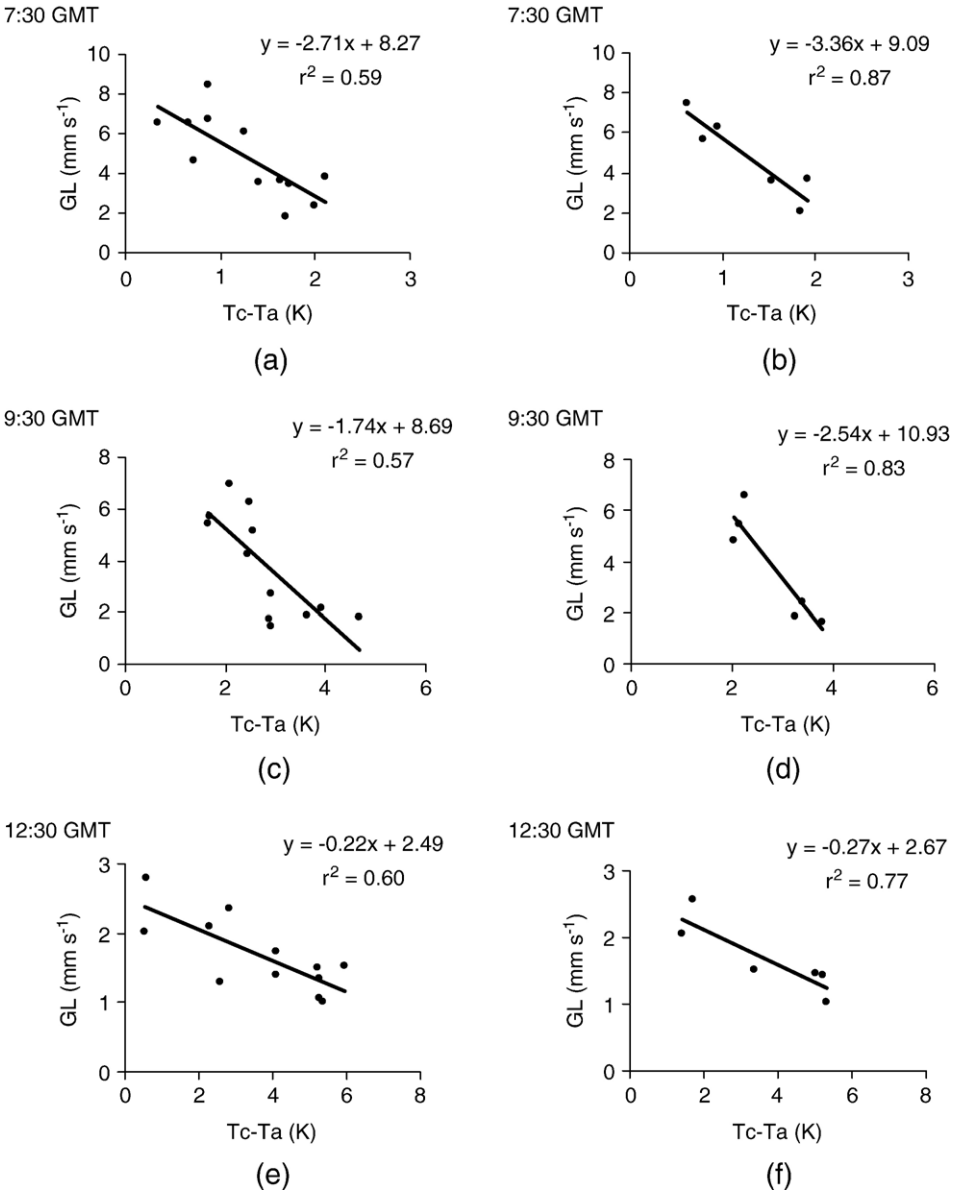

Fig. 7. Relationships between Tc–Ta (K) obtained with the AHS imagery and stomatal conductance (Gl) for olive trees. The relationship is for individual trees: a) at 7:30 GMT, c) at 9:30 GMT, and e) at 12:30 GMT; and for plots comprising 12 trees across 3 crop lines under the same irrigation level: b) at 7:30 GMT, d) at 9:30 GMT, and f) at 12:30 GMT.

treatments (B and D) yielded 1 K at 13:00 GMT in 2005, and Tc–Ta was 4 K for the B treatment and 3 K for D treatment (Table 5). These results demonstrate that airborne thermal imagery at high-spatial resolution is able to detect differences in tree crown temperature associated with irrigation levels, even within the range of variation of commercial irrigation doses applied in the peach orchard.

The assessment of the relationship between remote sensing-estimated crown tree temperature and field-measured stomatal conductance (Gl) and stem water potential (SWP) was specifically conducted on the olive tree orchard in the 2005 campaign at each of the three overflight times (water potential and conductance were measured on trees at each flight time). Fig. 7 shows the relationships between crown Tc–Ta, with Tc obtained with the airborne AHS thermal imagery, and the Gl measured in the field at 7:30 GMT (a, b), 9:30 GMT (c, d), and 12:30 GMT (e, f). The assessment was conducted for individual trees (Fig. 7a, c, e) and for experimental plots (12 trees) under the same irrigation treatment (Fig. 7b, d, f). Results yielded determination coefficients $r^2=0.59$ (7:30 GMT), $r^2=0.57$ (9:30 GMT), and $r^2=0.60$ (12:30 GMT) for individual trees; and determination coefficients of $r^2=0.87$ (7:30 GMT), $r^2=0.83$

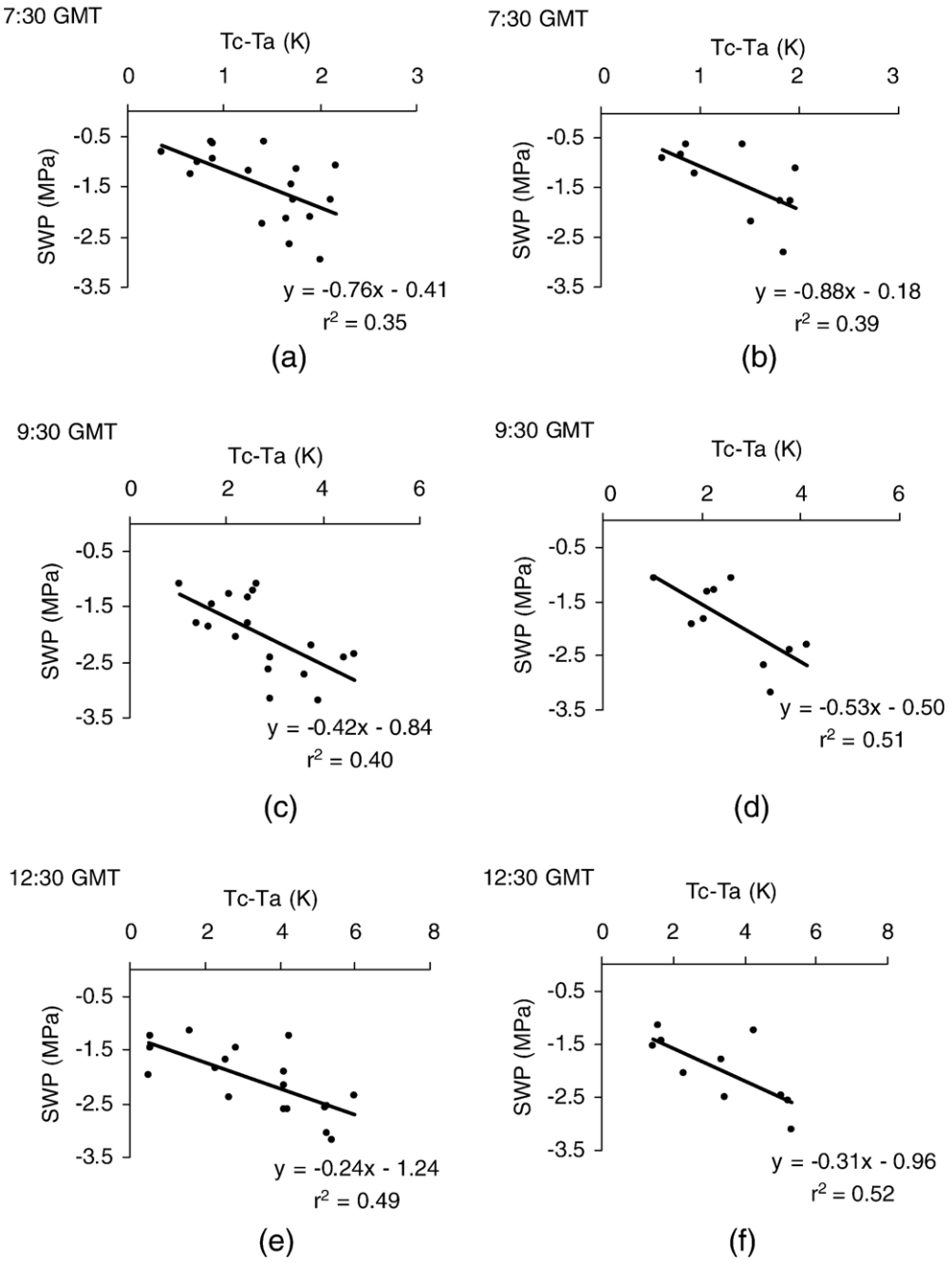

Fig. 8. Relationships between Tc–Ta obtained with the AHS imagery and stem water potential (SWP) measured in olive trees. For individual trees: a) at 7:30 GMT, c) at 9:30 GMT, and e) at 12:30 GMT and for plots comprising 12 trees across 3 crop lines under the same irrigation level: b) at 7:30 GMT, d) at 9:30 GMT, and f) at 12:30 GMT.

(9:30 GMT), and $r^2=0.77$ (12:30 GMT) for plots. Moreover, Fig. 8 shows the relationships obtained between SWP and Tc–Ta at each flight time. Determination coefficients yielded $r^2=0.35$ (7:30 GMT), $r^2=0.4$ (9:30 GMT), and $r^2=0.49$ (12:30 GMT) for individual trees; and $r^2=0.39$ (7:30 GMT), $r^2=0.51$ (9:30 GMT) and $r^2=0.52$ (12:30 GMT) for plots of 12 trees under the same irrigation treatment.

Analogously, Fig. 9 displays the results for the peach orchard, showing the relationships obtained between SWP and airborne remote sensing Tc–Ta estimated from the AHS imagery for individual trees (Fig. 9a, c, e) and for each irrigation treatment (Fig. 9b, d, f) for 2004 (a, b) and 2005 (c, d, e, f) campaigns. Results indicated the successful detection of water stress induced from orchard irrigation levels by airborne thermal imagery, obtaining determination coefficients between SWP and Tc–Ta of $r^2=0.81$ (9:00 GMT) in 2004, and $r^2=0.75$ (9:00 GMT) in 2005, for irrigation treatments. These results are consistent with those obtained for olive trees showing the capability of detecting orchard water stress as function of canopy temperature, even in the case of the peach orchard irrigated under commercial levels. The largest temperature differences among irrigation treatments for olive trees were obtained at 12:30 GMT image.

In order to study the feasibility of using medium resolution satellite sensors such as ASTER for water stress detection in open-tree canopies, a simulation of the ASTER sensor characteristics was conducted. The results of simulating the spectral characteristics of the ASTER sensor, aggregating crown, soil and shadow components at the treatment level (15×20 m^2

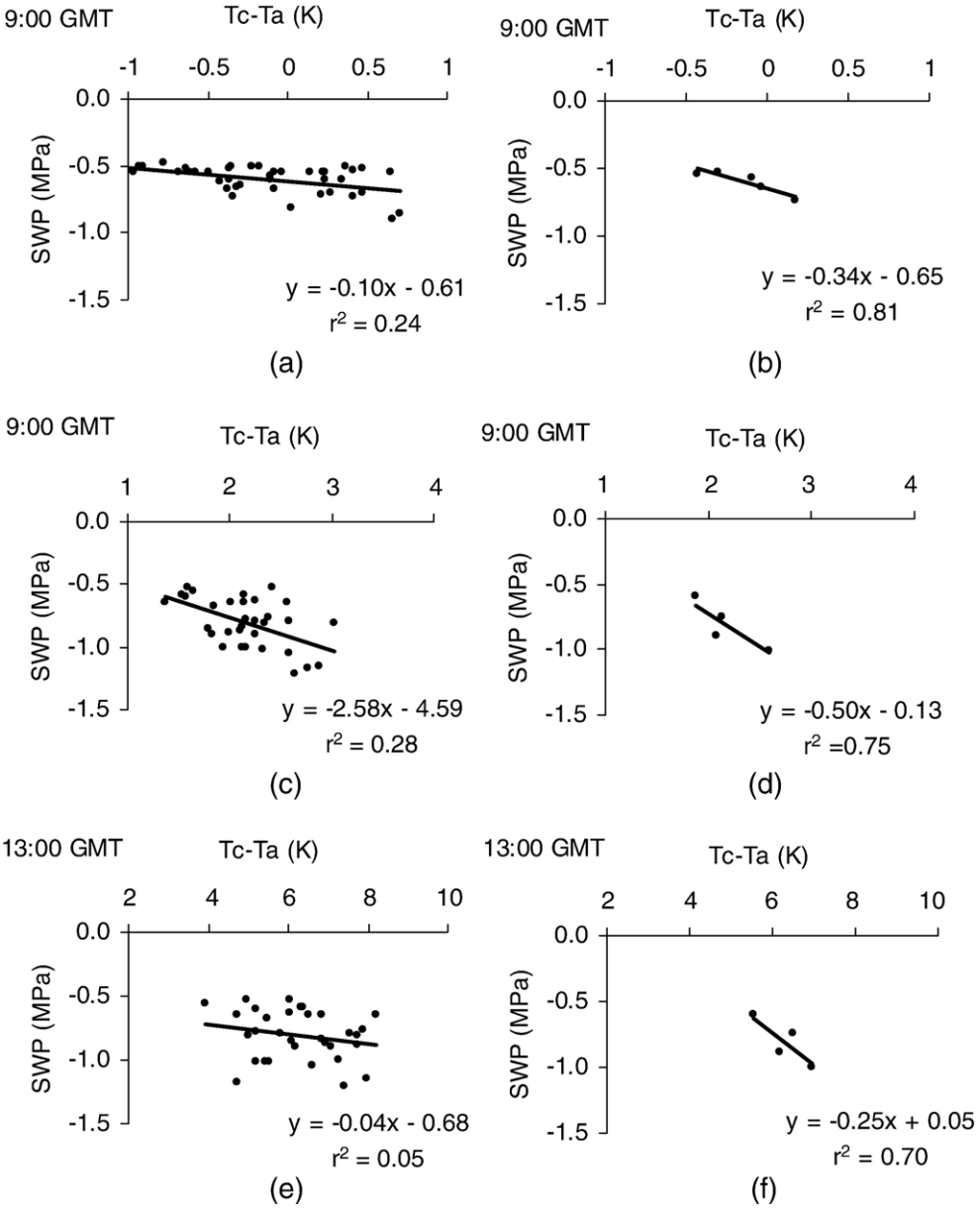

Fig. 9. Relationships between Tc–Ta values for peach trees estimated from the AHS imagery and stem water potential (SWP), for individual trees: a) at 9:00 GMT obtained in 2004, c) at 9:00 GMT obtained in 2005, and e) at 13:00 GMT obtained in 2005; and for irrigation treatments: b) at 9:00 GMT obtained in 2004, d) at 9:00 GMT obtained in 2005, and f) 13:00 GMT obtained in 2005.

spatial resolution due to the experimental design) are showed in the Fig. 10. Fig. 10 (a, c, and e) show the relationship between the land surface temperatures for treatment blocks of 15×20 m^2 obtained by the AHS sensor and simulated for the spectral characteristics of the ASTER sensor. The determination coefficients obtained were higher than $r^2=0.90$ at the three overflight times, yielding RMSE lower than 1 K (RMSE=0.04 at 9:30, RMSE=0.98 at 11:30 and RMSE=0.06 at 12:30 GMT). Fig. 10 (b, d, f) show the relationship obtained between the ASTER simulated canopy minus air temperature and SWP aggregated for the trees under the treatment block. The determination coefficients obtained were: $r^2=0.54$ (7:30 GMT) and $r^2=0.58$ (12:30 GMT). As compared with results obtained from AHS for treatment blocks between Tc–Ta and SWP (Fig. 8b, f), the determination coefficients were maintained in the ASTER simulation when the pixels were aggregated of pure crowns, soil

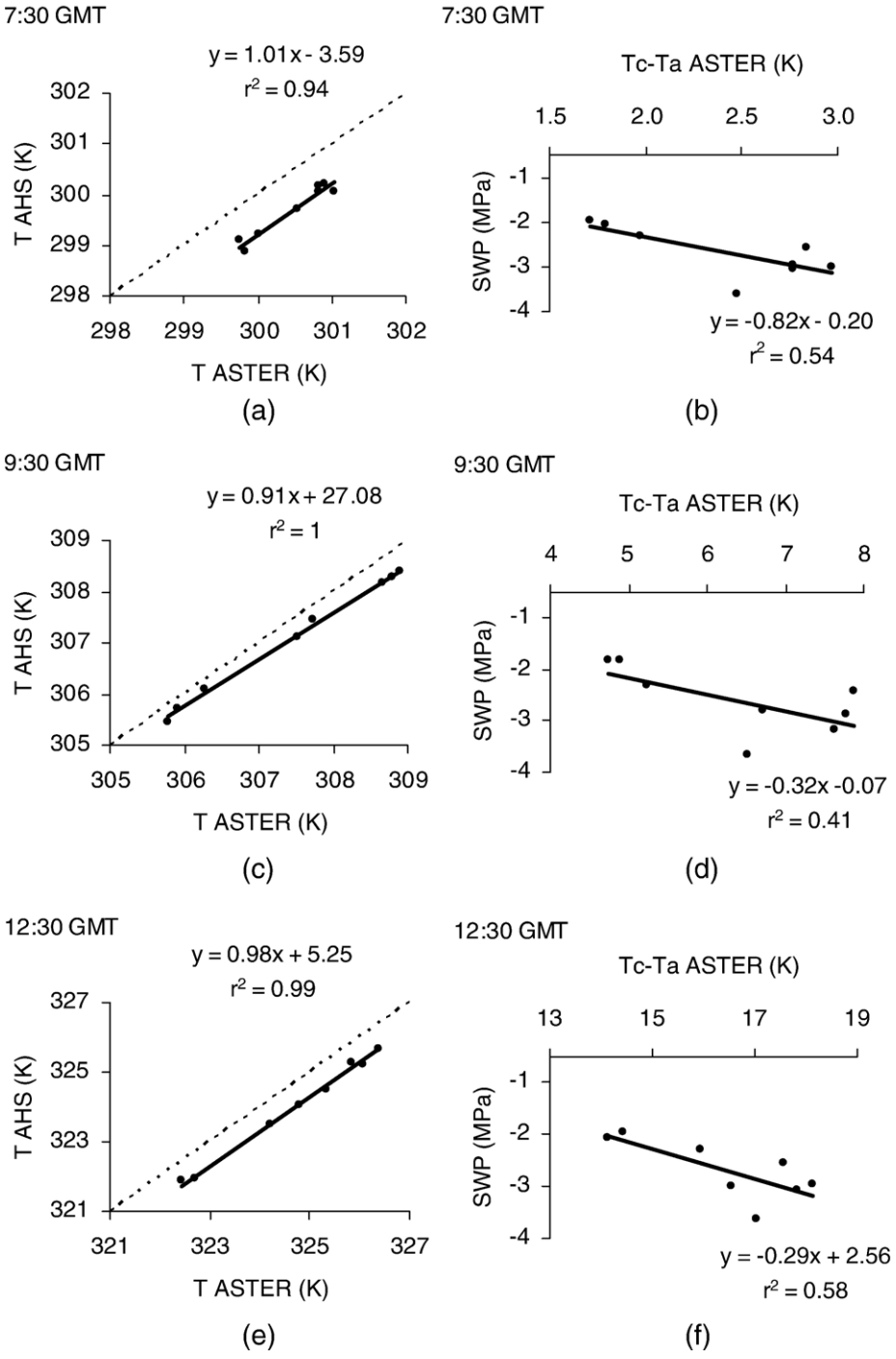

Fig. 10. Relationship between surface temperature of the 15×20 m^2 irrigation treatment blocks, obtained with the AHS sensor and simulated for the ASTER sensor characteristics: a) at 7:30 GMT, c) at 9:30 GMT and e) at 12:30 GMT. Relationships between Tc–Ta simulated for the ASTER characteristics and stem water potential: b) at 7:30 GMT, d) at 9:30 GMT, and f) at 12:30 GMT.

and shadows. These results suggest a potential application of these methods for water stress detection in open crop canopies with medium resolution sensors, showing that the small temperature differences as function of water stressed are not removed due to the soil and shadow effects in these open canopies. Although there was a mean temperature difference between vegetation (tree crowns) and sunlit soil of 11 K at 9:30 and 23 K at 12:30 (Table 6), the background temperature within each experimental plot was similar for all treatment plots due to the uniformity of the orchard soil and its management.

Finally, maps of the Tc–Ta difference were obtained for the peach tree orchard at two overflight times in 2005 (Fig. 11). The spatial distribution of the effects of the water stress in the canopy temperature in the orchard can be observed, as well as the temporal variation over the course of the day. It can be noticed how while most of the canopy did not surpass 2 K for Tc–Ta at 9:00 GMT, most of the canopy exceeded 5 K at 13:00 GMT. These maps of the spatial distribution of the water stress as function of canopy temperature in orchards may be very useful in the irrigation management using remote sensing imagery.

3.3. Remote sensing thermal imagery as an indicator of crop yield and fruit quality

The successful detection of water stress as function of irrigation levels in both the experimental olive field and the commercial peach orchard enabled the assessment of the orchard spatial variability and mapping of potential indicators of yield and some quality parameters. If irrigation doses affect some fruit quality parameters, remote-sensing estimates of thermal crown status should provide a tool for mapping within-field areas of potential homogeneous quality parameters at the tree scale. Such assessment was conducted with field-measured yield and fruit quality parameters from both olive and peach orchards.

Table 7 shows the determination coefficients obtained between remote sensing imagery Tc–Ta and yield and quality parameters in olive, such as olive yield, oil content (over dry fruit weight), fruit water content, oil yield and fruit fresh weight, in 2004 and 2005 campaigns. These relationships were obtained for plots of 12 trees under the same irrigation treatment (16 plots, four per treatment) and for the mean values of the different irrigation treatments, at the three overflight times (Table 7). Determination coefficients obtained per irrigation treatments for some olive quality parameters suggested a consistent relationship with water stress detected with thermal imagery: $r^2=0.95$ and $r^2=0.89$ for fruit water content, and $r^2=0.91$ and $r^2=0.92$ for fruit fresh weight, for 2004 and 2005 respectively. Table 7 shows worse relationships between Tc–Ta and yield and quality parameters for 2005 season. This can be explained by the alternate bearing habit of the olive trees, being 2005 an "off" year with 30% of the yield obtained in 2004.

Table 6
Mean temperatures obtained for pure vegetation, sunlit soil and shadows in the olive trees study site for each image collected on 16 July 2005

	Vegetation temperature (K)	Sunlit soil temperature (K)	Shadow temperature (K)
7:30 GMT	300.0±0.5	304.5±0.6	300.7±0.9
9:30 GMT	304.0±1.3	315.0±3.0	305.4±1.4
12:30 GMT	313.3±1.3	336.3±1.7	324.0±4.0

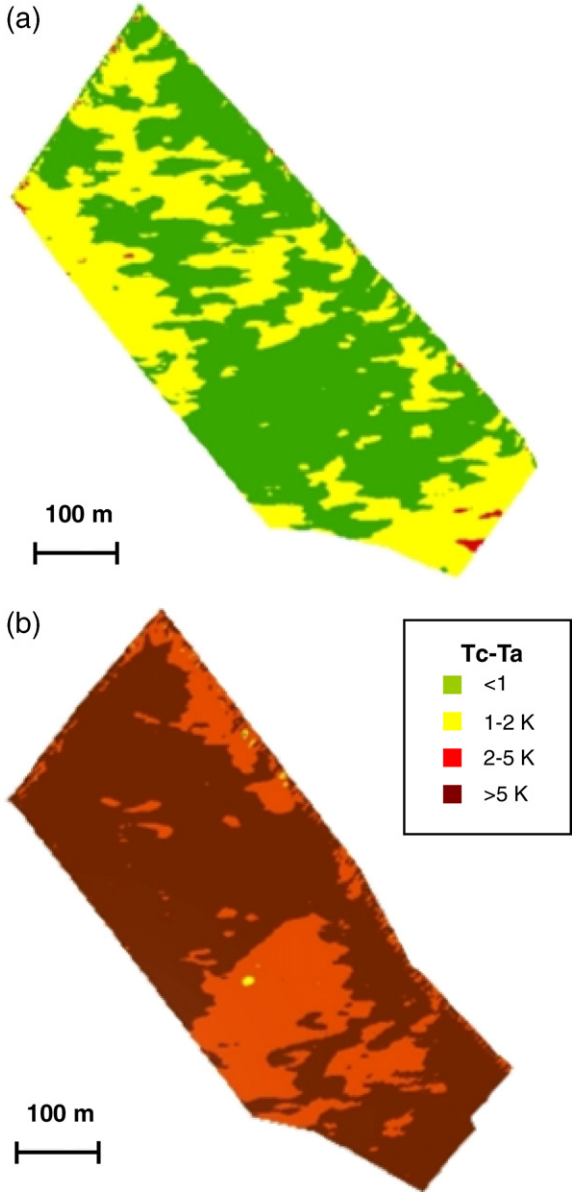

Fig. 11. Maps of the Tc–Ta difference of the peach orchard for the two overflight times in 2005: a) at 9:00 GMT, and b) at 13:00 GMT.

Similarly, Tc–Ta difference obtained from the AHS imagery (on 25 July 2004 and on 16 July 2005) was related with yield and some fruit quality parameters in peach trees. The assessment was conducted for data obtained in 2004 and 2005 (Table 8). Determination coefficients obtained per irrigation treatments from 2004 and 2005 campaigns also suggest the potential relationship between tree water stress detection with thermal imagery and peach quality indicators: $r^2=0.94$ and 0.77 for fruit mean diameter, $r^2=0.82$ and 0.81 for fruit weight, and $r^2=0.90$ and 0.83 for TSS content, for 2004 and 2005 respectively.

Table 7
Determination coefficients (r^2) obtained for the relationships between canopy minus air temperature (Tc–Ta) and yield and some quality parameters in olive for the plots of 12 trees under the same irrigation and for the irrigation treatments, obtained in 2004 and 2005 campaigns (significant values at $p<0.05$)

	r^2	Olive yield (kg tree^{-1})	Water content (%)	Oil content (%, per dry weight)	Oil yield (kg tree^{-1})	Fruit weight (g)
Tc–Ta (2004)	Plots 9:30 ($n=16$)	0.31	0.33	–	–	–
	Treatments 9:30 ($n=4$)	0.84	0.83	0.80	–	–
	Plots 11:30 ($n=16$)	0.39	0.69	–	–	0.53
	Treatments 11:30 ($n=4$)	0.77	0.95	–	–	0.91
	Plots 14:30 ($n=16$)	–	0.51	–	–	0.46
	Treatments 14:30 ($n=4$)	–	–	0.80	–	–
Tc–Ta (2005)	Plots 9:30 ($n=16$)	–	–	–	–	–
	Treatments 9:30 ($n=4$)	–	–	–	–	0.77
	Plots 11:30 ($n=16$)	–	–	–	–	–
	Treatments 11:30 ($n=4$)	–	–	–	–	0.92
	Plots 14:30 ($n=16$)	–	–	–	–	–
	Treatments 14:30 ($n=4$)	–	0.89	–	0.87	–

– No significant determination coefficients at $p<0.05$.
The imagery was taken on 25 July 2004 and 16 July 2005 at three times (9:30, 11:30 and 14:30 GMT).

Even though it is far fetched to estimate fruit quality parameters from simple relationships, our results suggest that high resolution thermal remote sensing can be used to infer some fruit quality parameters, as function of the water stress that can be detected at the single tree level. A single remote sensing image collected before harvest may provide useful information about tree water status in the orchard, and be used as an indicator for yield and fruit quality forecasting of the trees as affected by irrigation.

4. Summary and conclusions

This study extends the results obtained in a previous water stress study conducted in olive trees (Sepulcre-Cantó et al., 2006) demonstrating that: i) remote sensing detection of mild water stress in a commercial peach orchard is feasible over treatments under deficit irrigation; and ii) there is potential for the application of thermal remote sensing as an indicator of some fruit quality parameters in open-canopy orchards. Results of the 2004 and 2005 field campaigns showed that canopy temperature, stem water potential and stomatal conductance varied with the irrigation treatments applied to olive and peach trees. Infrared thermal sensors and thermal cameras were able to detect the temperature differences induced by water stress, even in the peach orchard, where only limited irrigation deficits were applied to avoid yield losses. In the olive trees, Tc–Ta yielded 6 K for trees under deficit irrigation and 5 K for trees under well irrigated treatment, while in the peach trees, Tc–Ta yielded up to 4 K for trees under deficit irrigation and 3 K for well irrigated trees in mid September, 2005. Field measurements with the thermal camera showed greater thermal homogeneity for the crown temperature in well-watered trees, obtaining a determination coefficient of $r^2=0.48$ between standard deviation of the imagery and the stem water potential. Results obtained from the AHS imagery showed at midday on 16 July 2005 differences in Tc–Ta between fully irrigated and stressed of 2 K for olive trees and 1 K for peach trees. These results show that AHS sensor was able to detect thermal differences between olive and peach trees under different deficit irrigation treatments. Determination coefficients between crown Tc–Ta obtained with the airborne AHS thermal imagery and olive tree stomatal conductance and stem water potential yielded $r^2=0.60$ (12:30 GMT) and $r^2=0.49$ (12:30 GMT) respectively, in 2005 for individual trees. These results suggest that temperature differences observed in trees under different irrigation treatments were due to water stress. Results on the peach orchard also showed successful detection of water stress as a function of mild water deficits imposed by different irrigation levels that were aimed at maintaining full commercial productivity. The determination coefficients between Tc–Ta obtained from the AHS imagery and stem water potential yielded $r^2=0.81$ (9:00 GMT). The results between the ASTER-simulated canopy minus air temperature

Table 8
Determination coefficients (r^2) for the relationships between canopy minus air temperature (Tc–Ta) and yield and some quality parameters in peach, obtained for plots under different irrigation treatments and for irrigation treatments obtained in 2004 and 2005 campaigns

	r^2	Number of fruits per tree	Yield (kg tree^{-1})	Diameter (mm)	Fruit weight (g)	Soluble solids content (%)
Tc–Ta (2004)	Plots ($n=16$)	0.34	0.32	0.24	–	–
	Treatments ($n=4$)	–	–	0.94	0.82	0.90
Tc–Ta (2005)	Plots ($n=16$)	–	0.33	0.41	0.44	0.43
	Treatments ($n=4$)	–	–	0.77	0.81	0.83

– No significant determination coefficients at $p<0.05$.
The imagery was collected on 25 July 2004 and 16 July 2005 at 9:00 GMT.

and stem water potential aggregated for the peach trees under the treatment block yielded $r^2=0.58$ (12:30 GMT). These results offer hope for applying these methods to ASTER satellite observations for global monitoring of open crop canopies.

This study focused on the potential of thermal remote sensing detection as a tool to quantify tree-level water stress and its relation to yield and fruit quality in olive and peach orchards. Determination coefficients for yield and some olive and peach quality parameters suggested a consistent relationship with remote sensing detected water stress, yielding $r^2=0.95$ (olive fruit water content) and $r^2=0.94$ (peach fruit mean diameter), at the treatment level. These results suggest that high resolution thermal remote sensing has potential as an indicator of yield and of some quality fruit parameters as affected by water stress that can be detected remotely at the single tree level. Maps of Tc−Ta could be used to assess the level of water deficits over orchards and to predict its impact on yield and fruit quality.

Acknowledgements

Financial support from the Spanish Ministry of Science and Education (MEC) for the projects AGL2003-01468, AGL2005-04049 and CONSOLIDER CSD2006-67 is gratefully acknowledged, as well as the support of grant from INIA (RTA02-070), DIMAS (INCO-CT-2004-509087) and CSIC (PIF-200440-F035). C. Ruz, J. Fortea, A. Gillespie, L. Balick and the GCU members M. Zaragoza, G. Soria, M. Romaguera and J. Cuenca are acknowledged for measurements and technical support in the field campaign. F. Villalobos, O. Pérez-Priego, L. Testi and I. Calatrava are acknowledged for scientific and technical support.

References

Abrams, M. (2000). The Advanced Spaceborne Thermal Emission and Reflection Radiometer (ASTER): Data products for the high spatial resolution imager on NASA's Terra platform. *International Journal of Remote Sensing*, *21*(5), 847−859.

Acevedo, E., Fereres, E., Hsiao, T., & Henderson, D. (1979). Diurnal growth trends, water potential, and osmotic adjustment of maize and sorghum leaves in the field. *Plant Physiology*, *64*, 476−480.

Berk, A., Anderson, G. P., Acharya, P. K., Chetwynd, J. H., Bernstein, L. S., Shettle, E. P., et al. (1999). *MODTRAN4 user's manual.* Hanscom AFB, MA: Air Force Research Laboratory.

Clawson, K. L., & Blad, B. L. (1982). Infrared thermometry for scheduling irrigation of corn. *Agronomy Journal*, *74*, 311−316.

Cohen, Y., Alchanatis, V., Meron, M., Saranga, Y., & Tsipris, J. (2005). Estimation of leaf potential by thermal imagery and spatial analysis. *Journal of Experimental Botany*, *56*, 1843−1852.

Cowan, I. R. (1965). Transport of water in the soil–plant–atmosphere system. *Journal of Applied Ecology*, *2*, 221−239.

Dash, P., Göttsche, F. M., Olesen, F. S., & Fischer, H. (2002). Land surface temperature and emissivity estimation from passive sensor data: Theory and practice current trends. *International Journal of Remote Sensing*, *23*(13), 2563−2594.

Detar, W. R., Penner, J. V., & Funk, H. A. (2006). Airborne remote sensing to detect water stress in full canopy cotton. *Transactions of the ASAE*, *49*(3), 655−665.

Fereres, E., Golhamer, D. A., & Parsons, L. R. (2003). Irrigation water management of horticultural crops. Historical review compiled for the American Society of Horticultural Science's 100th Anniversary. *Horticultural Science*, *38*(5), 1036−1042.

Fereres, E., & Soriano, A. (in press). Deficit Irrigation for Reducing Agricultural Water Use. *Journal of Experimental Botany.* doi:10.1093/jxb/erl165

Gao, B. C. (1996). NDWI a normalized difference water index for remote sensing of vegetation liquid water from space. *Remote Sensing of Environment*, *58*, 257−266.

Gao, B. C., & Goetz, A. F. H. (1995). Retrieval of equivalent water thickness and information related to biochemical components of vegetation canopies from AVIRIS data. *Remote Sensing of Environment*, *52*, 155−162.

Gillespie, A. R., Rokugawa, S., Hook, S., Matsunaga, T., & Kahle, A. B. (1998). A temperature and emissivity separation algorithm for Advanced Spaceborne Thermal Emission and Reflection Radiometer (ASTER) images. *IEEE Transactions on Geoscience and Remote Sensing*, *36*, 1113−1126.

Girona, J., Mata, M., Arbones, A., Alegre, S., Rufat, J., & Marsal, J. (2003). Peach tree response to single and combined regulated deficit irrigation regimes under shallow soils. *Journal of the American Society for Horticultural Science*, *128*(3), 432−440.

Harris, A., Bryant, R. G., & Baird, A. J. (2005). Detecting near-surface moisture stress in *Sphagnum* spp. *Remote Sensing of Environment*, *97*, 371−381.

Hidalgo, F. J., & Zamora, R. (2003). Edible oil analysis by high-resolution nuclear magnetic resonance spectroscopy: Recent advances and future perspectives. *Trends in Food Science & Technology*, *14*, 499−506.

Hsiao, T. C. (1973). Plant responses to water stress. *Annual Review of Plant Physiology*, *24*, 519−570.

Hsiao, T. (1990). Fisiología General. Vol. 1. In Curso Internacional Manejo de Agua en Frutales. Universidad de Concepción, Facultad de Ciencia Agronómicas, Veterinarias y Forestales, Departamento de Ingeniería Agrícola, Chillán, Chile.

Hsiao, T. C., Acevedo, E., Fereres, E., & Henderson, D. W. (1976). Stress metabolism. Water stress, growth and osmotic adjustment. *Philosophical Transactions of the Royal Society of London. B*, *273*, 479−500.

Idso, S. B., Jackson, R. D., Pinter, P. J., Reginato, R. J., & Hatfield, J. L. (1981). Normalizing the stress-degree-day parameter for environmental variability. *Agricultural and Forest Meteorology*, *24*, 45−55.

Idso, S. B., Jackson, R. D., & Reginato, R. J. (1978). Extending the "degree day" concept of phenomenological development to include water stress effects. *Ecology*, *59*, 431−433.

Jackson, R. D., Idso, S. B., Reginato, R. J., & Pinter Jr., P. J. (1981). Canopy temperature as a crop water stress indicator. *Water Resources Research*, *17*, 1133−1138.

Jackson, R. D., & Pinter Jr., P. J. (1981). Detection of water stress in wheat by measurement of reflected solar and emitted thermal IR radiation. *Spectral signatures of objects in remote sensing* (pp. 399−406). Versailles, France: Institut National de la Recherche Agronomique.

Jackson, R. D., Reginato, R. J., & Idso, S. B. (1977). Wheat canopy temperature: A practical tool for evaluating water requirements. *Water Resources Research*, *13*, 651−656.

Jang, J. D., Viau, A. A., & Anctil, F. (2006). Thermal-water stress index from satellite images. *International Journal of Remote Sensing*, *27*(8), 1619−1639.

Kerr, Y. H., Lagouarde, J. P., Nerry, F., & Ottlé, C. (2004). Land surface temperature retrieval techniques and applications: Case of AVHRR. In D. A. Quattrochi, & J. C. Luvall (Eds.), *Thermal remote sensingLand Surface Processes*. (pp. 33−109) Florida, USA: CRC Press.

Kramer, P. J., & Boyer, J. S. (1995). *Water relations of plants and soils.* San Diego, CA, USA: Academic Press.

Leinonen, I., & Jones, H. G. (2004). Combining thermal and visible imagery for stimulating canopy temperature and identifying plant stress. *Journal of Experimental Botany*, *55*, 1423−1431.

Mitchell, P. D., & Chalmers, D. J. (1982). The effect of reduced water supply on peach tree growth and yields. *Journal of the American Society for Horticultural Science*, *107*, 853−856.

Moran, M. S., Clarke, T. R., Inoue, Y., & Vidal, A. (1994). Estimating crop water deficit using the relation between surface-air temperature and spectral vegetation index. *Remote Sensing of Environment*, *46*, 246−263.

Moriana, A., Orgaz, F., Pastor, M., & Fereres, E. (2003). Yield responses of a mature olive orchard to water deficits. *Journal of the American Society for Horticultural Science*, *128*(3), 425−431.

Peñuelas, J., Fiella, I., Biel, C., Serrano, L., & Save, R. (1993). The reflectance at the 950–970 nm region as an indicator of plant water status. *International Journal of Remote Sensing*, *14*, 1887−1905.

Peñuelas, J., Pinol, J., Ogaya, R., & Fiella, I. (1997). Estimation of plant water concentration by the reflectance water index WI (R900 /R970). *International Journal of Remote Sensing*, *18*, 2869−2875.

Rock, B. N., Vogelmann, J. E., Williams, D. L., Vogelmann, A. F., & Hoshizaki, T. (1986). Remote detection of forest damage. *Bioscience*, *36*, 439−445.

Sepulcre-Cantó, G., Zarco-Tejada, P. J., Jiménez-Muñoz, J. C., Sobrino, J. A., de Miguel, E., & Villalobos, F. J. (2006). Within-field thermal variability detection as function of water stress in *Olea europaea* L. orchards with high spatial remote sensing imagery. *Agricultural and Forest Meteorology*, *136*, 31−44.

Serrano, L., Ustin, S. L., Roberts, D. A., Gamon, G. A., & Penuelas, J. (2000). Deriving water content of chaparral vegetation from AVIRIS data. *Remote Sensing of Environment*, *74*, 570−581.

Shackel, K. A., Ahmadi, H., Biasi, W., Buchner, R., Goldhamer, D., Gurusinghe, S., et al. (1997). Plant waterstatus as an index of irrigation need in deciduous fruit trees. *HortTechnology*, *7*, 23−29.

Slatyer, J. O. (1967). *Plant-water relationships.* New York: Academic press.

Sobrino, J. A., Jiménez-Muñoz, J. C., Zarco-Tejada, P. J., Sepulcre-Cantó, G., & de Miguel, E. (2006). Land surface temperature derived from airborne hyperspectral scanner thermal infrared data. *Remote Sensing of Enviroment*, *102*, 99−115.

Sobrino, J. A., Li, Z. L., Soria, G., & Jiménez, J. C. (2002). Land surface temperature and emissivity retrieval from remote sensing data. *Recent Research Developments on Geophysics*, *4*, 21−44.

Stimson, H., Breshears, D., Ustin, S., & Kefauver, S. (2005). Spectral sensing of foliar water conditions in two co-occurring conifer species: *Pinus edulis* and *Junisperus monosperma*. *Remote Sensing of Environment*, *96*, 108−118.

Uriu, K., & Magness, J. R. (1967). Deciduous tree fruits and nuts. In R. M. Hagan, H. R. Haise, & T. W. Edminster (Eds.), *Irrigation of agricultural landsMonograph*, *Vol. 11*. Madison, WI: American Society of Agronomy.

Ustin, S. L., Roberts, D. A., Pinzon, J., Jacquemoud, S., Gardner, M., Scheer, G., et al. (1998). Estimating canopy water content of chaparral shrubs using optical methods. *Remote Sensing of Environment*, *65*, 280−291.

Wanjura, D. F., Maas, S. C., Winslow, D. R., & Upchurch, D. R. (2004). Scanned and spot measured canopy temperatures of cotton and corn. *Computers and Electronics in Agriculture*, *44*(1), 33−48.

Yamaguchi, Y., Kahle, A. B., Tsu, H., Kawakami, T., & Pniel, M. (1998). Overview of Advanced Spaceborne Thermal Emission and Reflection Radiometer (ASTER). *IEEE Transactions on Geoscience and Remote Sensing*, *36*(4), 1062−1071.

Zarco-Tejada, P. J., Rueda, C. A., & Ustin, S. L. (2003). Water content estimation in vegetation with MODIS reflectance data and model inversion methods. *Remote Sensing of Environment*, *85*, 109−124.